1000 *Chem. Mater.* **2011,** *23,* 1000–1008
DOI:10.1021/cm102930z

CHEMISTRY OF MATERIALS
Article

Synthesis and Characterization of One-Dimensional Cr_2O_3 Nanostructures

Alexander C. Santulli,[†] Mikhail Feygenson,[‡] Fernando E. Camino,[§] M.C. Aronson,[‡,⊥] and Stanislaus S. Wong*[,†,‡]

[†]*Department of Chemistry, State University of New York at Stony Brook, Stony Brook, New York 11794-3400, United States,* [‡]*Condensed Matter Physics and Materials Science Department, Building 480, Brookhaven National Laboratory, Upton, New York 11973, United States,* [§]*Center for Functional Nanomaterials, Building 735, Brookhaven National Laboratory, Upton, New York 11973, United States, and* [⊥]*Department of Physics and Astronomy, State University of New York at Stony Brook, Stony Brook, New York 11794-3800, United States*

Received October 11, 2010

Herein, we report the synthesis of one-dimensional chromium oxide nanostructures, utilizing a modified sol−gel technique combined with a constrained template environment. Using scanning electron microscopy (SEM), transmission electron microscopy (TEM), and high-resolution transmission electron microscopy (HRTEM), we noted that individual nanowires were cylindrical in nature and appeared to be composed of smaller, crystalline, constituent nanoparticles, sintered and aggregated together so as to form a discrete, polycrystalline structure. Spectroscopic and diffraction investigations of our nanostructures confirmed their chemical composition with little if any impurities. Moreover, we further investigated the properties of our nanomaterials using both electrical and magnetic characterization. Interestingly, the magnetic properties of our nanostructures are strongly modified as compared with the bulk, due to the emergence of a net magnetic moment induced by uncompensated surface spins. Catalysis data showed that these nanostructures were active toward the thermal decomposition of $KClO_4$.

Introduction

Chromium sesquioxide or Cr_2O_3 is an important refractory material (due to its high melting temperature of ∼2435 K and oxidative resistance).[1,2] As such, it has found usage for coatings[3,4] known for their wear resistance and thermal protection,[5] solar energy collectors, and liquid crystal displays,[6] as well as for heterogeneous catalysts (e.g., hydrogenation and dehydrogenation of selected olefins, methanol synthesis, and SO_2 oxidation).[7−12] Interestingly, particles smaller than 50 nm have been used as transparent colorants.[5] Moreover, Cr_2O_3 is a wide band gap ($E_g \sim 3.4$ eV) *p*-type semiconductor (especially at lower temperatures) with potential applicability in optical and electronic devices and shows high electrical conductivity with reasonable levels of electron transfer.[13] Furthermore, bulk chromium sesquioxide is an antiferromagnetic material with a Néel temperature of 307 K;[14−16] however, in nanoscale Cr_2O_3, the observed magnetic properties are primarily driven by the presence of uncompensated surface spins.[17] Because it is also sensitive to hydrogen adsorption,[18] not surprisingly, Cr_2O_3 has also been used as a component of gas sensors for ethanol and ammonia vapor, operating through detectable electrical changes that can be probed by means of ac impedance spectroscopy and work function measurements.[19,20]

The need for nanoscale formulations of this material is 2-fold. First, high surface-area[7] Cr_2O_3 is required for many of their desirable applications, and commercial bulk Cr_2O_3 is

*To whom correspondence should be addressed. Phone: 631-632-1703; 631-344-3178. E-mail: sswong@notes.cc.sunysb.edu; sswong@bnl.gov.

(1) Ocana, M. *J. Eur. Ceram. Soc.* **2001**, *21*, 931–939.
(2) Kim, D. *Mater. Lett.* **2004**, *58*, 1894–1898.
(3) Bhushan, B.; Theunissen, G. S.; Li, X. *Thin Solid Films* **1997**, *311*, 67–80.
(4) Chatterjee, M.; Siladitya, B.; Ganguli, D. *Mater. Lett.* **1995**, *25*, 261–263.
(5) Tsuzuki, T. *Acta Mater.* **2000**, *48*, 2795–2801.
(6) Music, S.; Maljkovic, M.; Popovic, S.; Trojko, R. *Croat. Chem. Acta* **1999**, *72*(4), 789–802.
(7) Znaidi, L.; Pommier, C. *Eur. J. Solid State Inorg. Chem.* **1998**, *35*, 405–417.
(8) Lazier, W. A.; Vaughen, J. V. *J. Am. Chem. Soc.* **1932**, *54*, 3080–3095.
(9) Weckhuysen, B. M.; Schoonheydt, R. A. *Catal. Today* **1999**, *51*, 223–232.
(10) Grybowska, B.; Sloczynski, J.; Grabowski, R.; Keromnes, L.; Wcislo, K.; Bobinska, T. *Appl. Catal., A* **2001**, *209*, 279–289.
(11) Thakuria, H.; Borah, B. M.; Das, G. *J. Mol. Catal. A: Chem.* **2007**, *274*, 1–10.
(12) Pradier, C. M.; Rodrigues, F.; Marcus, P.; Landau, M. V.; Kaliya, M. L.; Gutman, A.; Herskowitz, M. *Appl. Catal., B* **2000**, *27*, 73–85.
(13) Cao, H.; Qiu, X.; Liang, Y.; Zhao, M.; Zhu, Q. *Appl. Phys. Lett.* **2006**, *88*(24), 241112/1–241112/3.
(14) Banobre-Lopez, M.; Vazquez-Vazquez, C.; Rivas, J.; Lopez-Qunitela, M. A. *Nanotechnology* **2003**, *14*, 318–322.
(15) Zhang, W. S.; Brueck, E.; Zhang, Z. D.; Tegus, O.; Li, W. F.; Si, P. Z.; Geng, D. Y.; Buschow, K. H. J. *Phys. B (Amsterdam, Neth.)* **2005**, *358*, 332–338.
(16) Stoner, S. *Phys. Rev.* **1963**, *130*, 183.
(17) Vollath, D. *Mater. Lett.* **1996**, *29*, 271–279.
(18) Burwell, R. L.; Taylor, H. S. *J. Am. Chem. Soc.* **1936**, *58*(5), 697–705.
(19) Pohkrel, S.; Simion, C. E.; Quemener, V.; Barsan, N.; Weimar, U. *Sens. Actuators, B* **2008**, *133*, 78–83.
(20) Liang, X.; Zhong, T.; Guan, H.; Liu, F.; Lu, G.; Quan, B. *Sens. Actuators, B* **2009**, *136*, 479–483.

Published on Web 01/07/2011

difficult to sinter. Second, the production of finely divided magnetic solids has been known to exhibit anomalous magnetic behavior for these materials relative to their bulk forms.[21] A number of disparate methods have been reported to synthesize Cr_2O_3 nanoparticles and aerogels, including but not limited to hydrothermal processing,[22,23] the use of supercritical fluids,[7,24] precipitation−gelation reactions,[2,4,25] a solid thermal decomposition reaction,[26] mechanochemical processing,[5] hydrazine reduction coupled with thermal treatment,[27] precursor calcination and annealing,[14,15] laser-induced deposition from solution,[28] laser-induced pyrolysis,[29] room-temperature sonochemical reduction,[30] forced hydrolysis from chromium precursors,[1,6] and microwave plasma processing.[17]

In contrast, there have been only relatively few previous reports pertaining to the synthesis of anisotropic, one-dimensional (1D) Cr_2O_3. For instance, Cr_2O_3 nanobelts have been synthesized using chemical vapor deposition[31] as a result of flowing ethanol vapor over a piece of Cr metal heated to 800 °C. Whereas as-produced uniform single-crystalline nanobelts were produced, the synthesis protocol necessitated the use of high temperatures in a controlled gaseous atmosphere (whose precise role in the formation mechanism of these nanostructures was not understood) and, moreover, yielded a relatively polydisperse product in terms of a size distribution (e.g., widths ranging from tens to hundreds of nanometers). A similar need for an excessive thermal treatment was evident in the preparation of Cr_2O_3 nanorods and nanowires, measuring 50 nm in diameter and 550 nm in length, generated through the annealing of precursor $Cr(OH)_3$ nanoparticles at temperatures higher than 1027 K.[32] In addition, Cr_2O_3 nanotubes with diameters of 80 nm and lengths of 550 nm have also been synthesized in a solvothermal reduction at 180 °C in the presence of acetyl acetone and ethylene glycol.[33]

A few groups have latched onto the idea of the use of different types of templates as a platform with which to facilitate one-dimensional growth. For example, calcination of hydrated precursors at 550−650 °C for 5 to 6 h within the straight, close-packed, porous channels of mesoporous silica[34,35] has been reported to yield single crystals of Cr_2O_3 nanowires. An analogous calcination[36] at 550 °C using multiwalled carbon nanotubes as a template via a supercritical fluid-mediated route has also been demonstrated to produce chromium oxide nanotubes. A third approach[13] reported immersion of pores of alumina templates in a $Cr(OH)_3$ sol, initially created using hydrazine, for 4 to 5 h under 1.3 atm at ambient temperature followed by annealing under an argon atmosphere to 600 °C for 5 h in order to yield nanowires in the range of 100−300 nm in diameter and over 10 μm in length.

Apart from the fact that we do not rely on the use of a microemulsion or an autoclave, the method we have reported herein for the synthesis of high-aspect-ratio Cr_2O_3 nanowires is distinctive from all of these previous experiments mentioned in several ways. First, we do not require the use of either specialized or inert gases during our annealing procedure, which can actually be run under air. Second, our procedure does not require any particular high-temperature annealing treatment in order to specifically isolate the product from within the template. In fact, our polycarbonate template platform is actually burned off as a normal byproduct of our synthesis steps. Third, while our specific method necessitates the application of pressure, its duration is much more rapid (30−45 min) as compared with previous reports, and overall, our reaction times are noticeably faster than those of previous groups. Fourth, while our procedure is based upon a sol−gel methodology, we have tried to simplify the process as much as possible. For example, we do not use hydrazine, supercritical fluids, or any particularly hazardous conditions in order to facilitate the reaction progression. We have demonstrated the catalytic behavior of our nanostructures herein for the destruction of $KClO_4$.

Moreover, we have also investigated the magnetic properties of our Cr_2O_3 nanowires. We find that, in as-prepared 1D Cr_2O_3 nanostructures, the magnetic properties are strongly modified as compared with the bulk, due to the emergence of a net magnetic moment induced by uncompensated surface spins, as has been previously reported for Cr_2O_3 nanoparticles.[14,15,37,38] Furthermore, previous reports have indicated the presence of an exchange bias effect in Cr_2O_3 nanoparticles,[15,38] as a result of the exchange coupling between the surface spins and core; we have sought an analogous effect for our samples herein.

Experimental Section

All chemicals were used as received without additional purification. Our methodology is based upon an adaptation of a sol−gel procedure that has been previously reported[25] for a generic synthesis of metal oxide aerogels using inorganic salt precursors.

(21) Balachandran, U.; Siegel, R. W.; Liao, Y. X.; Askew, T. R. *Nanostruct. Mater.* **1995**, *5*(5), 505–512.
(22) Pei, Z.; Xu, H.; Zhang, Y. *J. Alloys Compd.* **2009**, *468*(1−2), L5–L8.
(23) Pei, Z.; Zhang, P. *Mater. Lett.* **2008**, *62*, 504–506.
(24) Abecassis-Wolfovich, M.; Rotter, H.; Landau, M. V.; Korin, E.; Erenburg, A. I.; Mogilyansky, D.; Gartstein, E. *J. Non-Cryst. Solids* **2003**, *318*, 95–111.
(25) Gash, A. *J. Non-Cryst. Solids* **2001**, *285*, 22–28.
(26) Li, L.; Yan, Z. F.; Lu, G. Q.; Zhu, Z. H. *J. Phys. Chem. B* **2006**, *110*, 178–183.
(27) Gui, Z.; Fan, R.; Mo, W.; Chen, X.; Yang, L.; Hu, Y. *Mater. Res. Bull.* **2003**, *38*, 169–176.
(28) Zhong, Z. C.; Cheng, R. H.; Bosley, J.; Dowben, P. A.; Sellmyer, D. J. *Appl. Surf. Sci.* **2001**, *181*, 196–200.
(29) Peters, G.; Jerg, K.; Schramm, B. *Mater. Chem. Phys.* **1998**, *55*, 197–201.
(30) Dhas, N. A.; Koltypin, Y.; Gedanken, A. *Chem. Mater.* **1997**, *9*, 3159–3163.
(31) Han, W.; Wu, L.; Stein, A.; Zhu, Y.; Misewich, J.; Warren, J. *Angew. Chem.* **2006**, *45*, 6554–6558.
(32) Wang, J.; Sun, J.; Bian, X. *Modell., Meas. Control, C* **2004**, *65* (1), 47–56.
(33) Yu-Feng, Z.; Zheng-Song, L.; Qian-Wang, C. *Chin. J. Inorg. Chem.* **2004**, *20*(8), 971–974.
(34) Tian, B.; Liu, X.; Yang, H.; Xie, S. Y., C.; Tu, B.; Zhao, D. *Adv. Mater.* **2003**, *15*(5), 1370–1374.
(35) Dickinson, C.; Zhou, W.; Hodgkins, R. P.; Shi, Y.; Zhao, D.; He, H. *Chem. Mater.* **2006**, *18*, 3088–3095.
(36) An, G.; Zhang, Y.; Liu, Z.; Miao, Z.; Han, B.; Miao, S.; Li, J. *Nanotechnology* **2008**, *19*(3), 035504/1–035504/7.
(37) Vazquez-Vaquez, C.; Banobre-Lopez, M.; Lopez-Quintanela, M. A.; Hueso, L. E.; Rivas, J. *J. Magn. Magn. Mater.* **2004**, *272*, 1547.
(38) Makhlouf, S. A. *J. Magn. Magn. Mater.* **2004**, *272*−*276*, 1530–1532.

Specifically, to the resulting aqueous, translucent, dark green solution of chromium chloride hexahydrate (Strem Chemicals) was added an aliquot of propylene oxide (Acros Organic, 99.5%) in a molar ratio of ~1:3.5 with thorough stirring. The purpose of the propylene oxide in the solution is to act as a gelation promoter.[25] Upon thorough mixing, droplets of the sol precursor solution were forced into the hollow pores of 6 μm thick porous Whatman polycarbonate track-etched membranes (containing 200 nm pore sizes) by systematic and continuous application of pressure through the mediation of a 25 mL syringe, until the template pore channels appeared to be fully saturated with solution, upon visual inspection. After cleaning of its external surface to dryness, the polycarbonate template was subsequently placed into a porcelain crucible (i.e., a glazed porcelain boat) and heated in air to 600 °C for 1 h at a ramp rate of 5 °C/min followed by natural cooling to room temperature. In additional experiments, we also used templates with nominal pore sizes of 100, 50, and 15 nm. Of significance, we should note that it has been previously shown for polycarbonate templates with pore sizes less than 100 nm that (i) the pore size is often not consistent throughout the full length of the template and (ii), hence, as-obtained nanowire diameters can be larger than expected by factors of as much as 2−4.[39,40]

Characterization. To prepare powder X-ray diffraction (XRD) samples, the resulting chromate nanorods were rendered into slurries in ethanol, sonicated for about 1 min, and then air-dried upon deposition onto glass slides. Diffraction patterns were collected using a Scintag diffractometer, operating in the Bragg-Bretano configuration using Cu Kα radiation (λ = 1.54 Å) from 20 to 70° at a scanning rate of 2° per minute.

Mid-infrared spectra were obtained on a Nexus 670 (Thermo Nicolet) equipped with a Smart Orbit accessory, a KBr beam splitter, and a deuterated triglycine sulfate (DTGS) KBr detector. As-prepared solid powder samples were placed onto a diamond crystal where data were taken with a reproducible pressure. A background correction was performed using the diamond crystal in the spectral range studied. UV−visible spectra were collected at high resolution on a Beckmann Coulter model DU 640 spectrometer using quartz cells with a 10 mm path length. Spectra were obtained for as-prepared samples, which were sonicated in distilled water so as to yield homogeneous dispersions. UV−visible absorption spectra were recorded using distilled water as a blank. We have also obtained analogous spectral data in ethanol, dimethylformamide (DMF), and cyclohexane with a series of nanowire concentrations ranging from <1 μg/mL to 0.5 mg/mL. Raman data were taken using a WiTec alpha 300 microscope using an excitation wavelength of 532 nm with a power of ~0.5 mW to avoid strong laser heating. Spectra were acquired with an integration time of 10 s with a total of 30 scans. Scattered light was analyzed using a 600 mm^{-1} spectrometer grating with a spectral resolution of ~3 cm^{-1}.

The diameters and lengths of as-prepared 200 nm diameter nanorods were initially characterized using a field emission scanning electron microscopy instrument (FE-SEM Leo 1550), operating at an accelerating voltage of 20 kV and equipped with energy-dispersive X-ray spectroscopy (EDS) capabilities. The corresponding diameters and lengths of as-prepared 100, 50, and 15 nm diameter nanorods were analyzed using a Hitachi S4800, operating at an accelerating voltage of 5 kV. Samples for SEM were prepared by dispersing as-prepared chromate nanorods in ethanol, sonicating for about 2 min, and then depositing several drops of the sample solution onto a silicon wafer, attached to a SEM aluminum stub.

High-resolution transmission electron microscopy (HRTEM) images and selected area electron diffraction (SAED) patterns were obtained on a JEOL 2010F instrument at accelerating voltages of 200 kV. Specimens for all of these TEM experiments were prepared by dispersing the as-prepared product in ethanol, sonicating for 2 min to ensure adequate dispersion of the nanowires, and dipping one drop of the solution onto a 300 mesh Cu grid, coated with a lacey carbon film.

To perform electrical characterization, Pt contacts were defined by ion beam assisted deposition using the Ga ions of a dual-beam SEM/focused ion beam (FIB) system. This fabrication method was chosen because our nanowires showed poor adhesion to substrates (600 nm SiO_2/n^+ Si) during the electrode metal lift-off stage of conventional e-beam lithography. Current−voltage ($C-V$) curves at different temperatures were measured for two nanowires (named A and B here) using a cryogenic probe station that spanned the 4−300 K temperature range. $C-V$ curves were Ohmic from 300 K down to 4 K as can be seen in the upper inset of Figure 4. Only curves at 4 K were slightly non-Ohmic.

In order to study the magnetic properties of Cr_2O_3 nanowires, we measured both the temperature and field dependence of direct current (dc) magnetization at a range from 10 to 320 K and in magnetic fields as large as 50 kOe, using a Quantum Design Magnetic Property Measurement System (MPMS-XL7) instrument. In a typical experiment, 3 mg of nanowires were contained in gelatin capsules and fastened in plastic straws for immersion into the magnetometer. No subtraction of the diamagnetic signal associated with the sample container was made for the magnetization data.

As part of our study of Cr_2O_3 reactivity, thermogravimetric analysis (TGA) was performed in a dry air environment using a TA Instruments Q500 TGA model. Experiments were carried out from room temperature to 700 °C with a heating rate of 5 °C/min. Samples of 3 to 4 mg were placed in a platinum pan for individual runs.

Results and Discussion

I. Synthesis and Structural Characterization. The purity and crystallinity of as-prepared chromium oxide nanorod samples were initially characterized using powder X-ray diffraction (XRD). All of the diffraction peaks observed from as-prepared samples in Figure 1A (top, red curve) can be readily ascribed to a rhombohedral-phase crystal structure with lattice constants of a = 4.922 Å and c = 13.62 Å, which are comparable to reported database values (Figure 1A, bottom, blue curve) of a = 4.958 Å and c = 13.58 Å for pure Cr_2O_3 bulk materials (JCPDS #85-0869; space group of R3c). We did not note any peaks that could be definitively ascribed to an impurity such as either a hydrated phase or a nonstoichiometric phase of our desired compound. We attribute this observation mainly to the complete high-temperature conversion and crystallization of the precursor gel into chromium oxide. Furthermore, the fact that the template used to create these nanomaterials is composed of polycarbonate implied that it could be completely burned off and removed in situ after heating to 600 °C as the product was forming. Because of this

(39) Schonenberger, C.; van der Zande, B. M. I.; Fokkink, L. G. J.; Henny, M.; Schmid, C.; Kruger, M.; Bachtold, A.; Huber, R.; Birk, H.; Staufer, U. *J. Phys. Chem. B* **1997**, *101*, 5497–5505.
(40) Tian, M.; Wang, J.; Jurtz, J.; Mallouk, T. E.; Chan, M. H. W. *Nano Lett*. **2003**, *3*(7), 919–923.

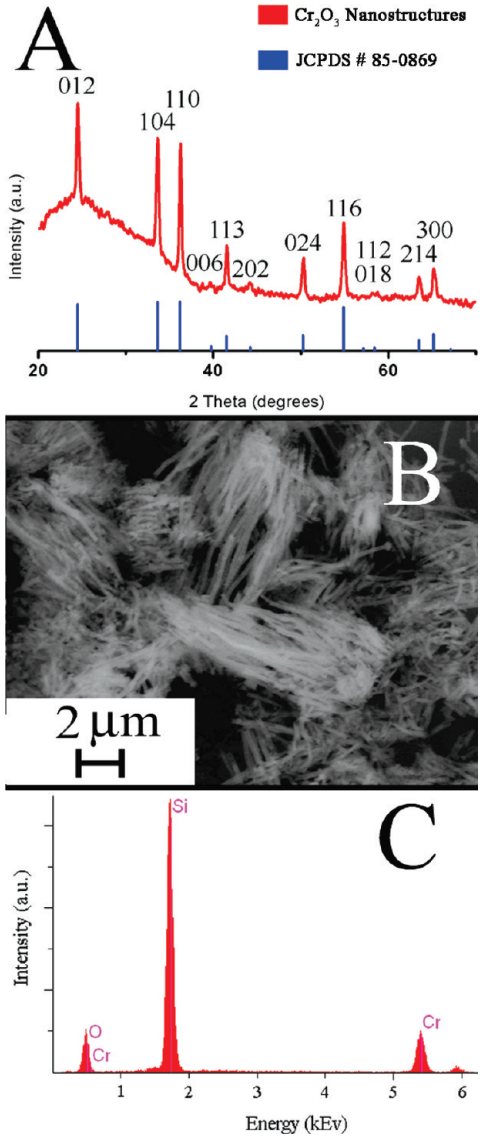

Figure 1. (A) Powder XRD of Cr_2O_3 nanowires. (B) Representative low-magnification SEM image of Cr_2O_3 nanowires. (C) EDS of sample shown in (B).

sintering process, the presence of any carbonaceous material should have been very minimal to none. Furthermore, apart from XRD, additional SEM and TEM characterization showed no evidence of the presence of any discernible amount of carbonaceous material that could be unambiguously ascribed to the template. Therefore, isolation of our product did not necessitate any additional separation or purification steps, unlike for other previously reported methods.[13] As a matter of note, the broad peak from 2θ values of 20 to 40° is associated with the amorphous glass slide used to support the sample.

Using FE-SEM, we were able to visualize our nanostructures so as to conclusively determine their final morphology. As can be seen from the SEM image shown in Figure 1B, as-obtained samples primarily consist of one-dimensional wirelike motifs with a small impurity consisting of isolated, unsupported nanoparticles, i.e., $< 10\%$ of the overall sample. That is, on average, there were 90% nanowires present in the sample. From additional experiments (Supporting Figure S1, Supporting Information), we note that both the nature and extent of the cleaning of the external template surface, prior to its heating, were directly correlated with the amount of isolated nanoparticles ultimately observed. Analysis suggested that the as-obtained nanowires measured 179 ± 29 nm in diameter, consistent with the size of the originating template pores (i.e., 200 nm) and that their lengths extended to several micrometers. Using templates with pore sizes of 100, 50, and 15 nm resulted in the production of polycrystalline nanowires with average widths of 143 ± 21, 87 ± 12, and 31 ± 5 nm, respectively (Supporting Figure S2, Supporting Information). However, we did not isolate enough of these nanowires to adequately compare the optomagnetic behavior of our nanostructures with the bulk. It is important to note that all of these 1D nanostructures are structurally robust, as they can withstand 30 min of sonication without evident disintegration noted. The corresponding EDS spectrum (Figure 1C) highlights the presence of only chromium and oxygen peaks, with no other relevant elements present; the large Si peak can be attributed to the Si wafer upon which the nanostructures were deposited prior to analysis. We should also state at this point that the subsequent magnetic and optoelectronic measurements were performed on the 200 nm diameter nanorod sample, because it was easiest to fabricate as pure, crystalline 1D motifs in relatively large quantities.

TEM images shown in Figure 2A,B clearly reinforce the view not only that the nanowires are relatively straight but also that their external surfaces are relatively roughened and irregular, as if they were composed of constituent substructure. Indeed, individual nanowires are cylindrical in nature and appear to be composed of smaller, constituent nanoparticles, sintered and aggregated together so as to form a discrete polycrystalline structure. This observation coupled with the nontrivial selected area electron diffraction pattern, shown as an inset to Figure 2A, also supports the idea of the overall polycrystallinity of our nanowires. Further evidence for this assertion is provided upon investigation of these nanowires at higher magnifications (Figure 2C) wherein the lattice planes of individual, constituent single-crystalline nanocrystals can be clearly observed. The most prominent lattice planes present have been indexed and correspond to the 012 and the 11−6 planes of the rhombohedral phase of chromium oxide (JCPDS #85-0869), consistent with our XRD results. In fact, the measured lattice distance for the 012 plane, in particular, was determined to be 0.374 ± 0.05 nm, which is only a 2% difference from the expected JCPDS value of 0.364 nm. It could be argued that our wirelike structures are composed of a string of adjoining individual single-crystalline nanocrystal components, each measuring 36 ± 17 nm in size, sintered together to form a 1D motif. These as-formed nanocrystals are interconnected and aligned onto the adjoining wire surface without the apparent and obvious presence of misorientations, though these certainly cannot be fully discounted. Our group has previously observed a very similar structural motif for

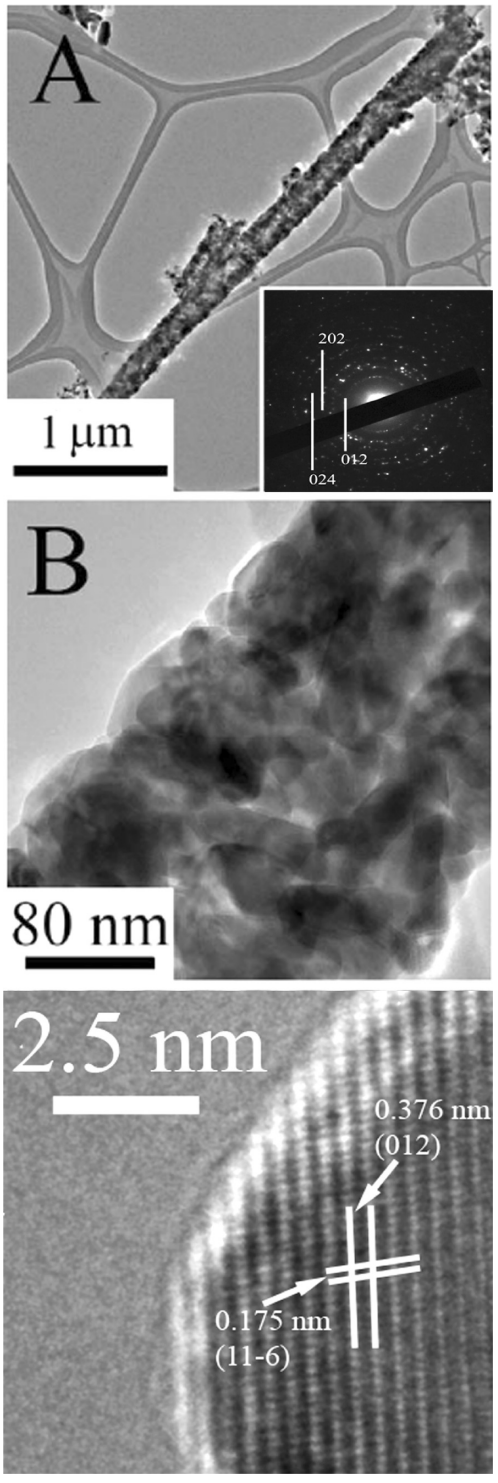

Figure 2. (A) Low-magnification TEM of a single Cr_2O_3 nanowire. Inset: selected area electron diffraction pattern of this nanowire. (B) Higher-magnification TEM image of nanowire presented in (A). (C) HRTEM image of an individual, crystalline constituent nanoparticle within the nanowire shown in (A). Lattice planes shown correspond to the (1−16) and (012) planes of Cr_2O_3.

anatase TiO_2 wires, ostensibly formed from the directed self-aggregation process of individual anatase TiO_2 nanocrystals.[41]

II. Opto-Electronic Properties. Subsequent spectroscopic analysis of our as-prepared nanowires further supported the notion that our nanowires are crystalline Cr_2O_3. Bands present in the infrared (IR) spectrum (Figure 3A) of our nanomaterials correspond reasonably well with those previously reported in the literature for bulk. For instance, the peaks in the region from 850 to 1100 cm^{-1} can be identified as various combination lattice modes. Specifically, peaks at 1092, 948, and 882 cm^{-1} can be ascribed to $E_2' + A_2'$, $E_2' + E_3'$, and 2 E_2' modes, respectively;[42] another group assigned the 1092 cm^{-1} band to a stretching vibration of Cr=O.[36] Additional peaks present at lower wavenumbers, namely at 609, 512, and 441 cm^{-1}, respectively, have been associated with the stretching vibrations of Cr−O of crystalline α-Cr_2O_3, in agreement with previous data,[1,7,36,43] and have been attributed to fundamental infrared-active vibrations, corresponding to E_4, E_3, and E_2 modes respectively.[42]

The UV−visible spectrum of the nanowires, dispersed in water, is shown in Figure 3B. While it is clearly a broad feature, there are noticeable shoulder peaks located at 378, 472, and 591 nm, respectively. These values correspond reasonably well with those reported in prior literature for chromium oxide species.[26,44−46] The peak centered at 378 nm has been previously associated either with Cr^{4+} ions[46] or with the O−Cr^{6+} charge transfer transition of chromate species with tetrahedrally coordinated Cr^{6+} ions,[44] suggesting their potential presence within the Cr_2O_3 nanostructures we have generated. The two remaining features at 472 and 591 nm have been ascribed to the intrinsic $^4A_{2\,g} \rightarrow {}^4T_{1\,g}$ and the $^4A_{2\,g} \rightarrow {}^4T_{2\,g}$ transitions of Cr^{3+} ions, localized within six-coordinate geometry and octahedral symmetry, respectively.[26] Data obtained in ethanol, DMF, and cyclohexane, at varying nanowire concentrations, were similarly broadened, an observation which has been previously ascribed to (a) light scattering due to the relatively large size of the nanowires, (b) the relatively low inherent solubility of the product, and (c) solvent dipole effects.[47] Moreover, it is important to note that the UV−visible spectra were taken on nanowires dispersed in suspensions, as opposed to true, optically transparent solutions of solubilized nanowires.

Figure 3C shows the Raman spectrum for our as-synthesized chromium oxide nanowires. Peaks present at 315, 355, 556, and 612 cm^{-1} for as-prepared nanowires are consistent with both our bulk data (Figure 3D) as well as with values reported in the literature.[48] In fact, the most intense peak centered around 556 cm^{-1} has been attributed to a

(41) Mao, Y.; Kanungo, M.; Hemraj-Benny, T.; Wong, S. S. *J. Phys. Chem. B* **2006**, *110*, 702–710.
(42) Ratnasamy, P.; Leonard, A. J. *J. Phys. Chem.* **1972**, *76*(13), 1838–1843.
(43) McDevitt, N. T.; Baun, W. L. *Spectrochim. Acta* **1964**, *20*, 799–808.
(44) Li, H.; Yue, Y.; Mao, C.; Zaiku, X.; Hua, W.; Zi, G. *Chin. J. Catal.* **2006**, *27*(1), 4–6.
(45) Weckhuysen, B. M.; Wachs, I. E.; Schoonheydt, R. A. *Chem. Rev.* **1996**, *96*, 3327–3349.
(46) Zhang, L. D.; Mo, C. M.; Cai, W. L.; Chen, G. *Nanostruct. Mater.* **1997**, *9*, 563–566.
(47) Willard, H. H.; Merritt, L. L.; Dean, J. A. *Instrumental methods of analysis*, 4th ed.; D. Van Nostrand Company, Inc.: 1965; p 80−90.
(48) Lin, C. H.; Shen, P.; Chen, S. Y. *Appl. Phys. B: Laser Opt.* **2010**, *98*, 443–450.

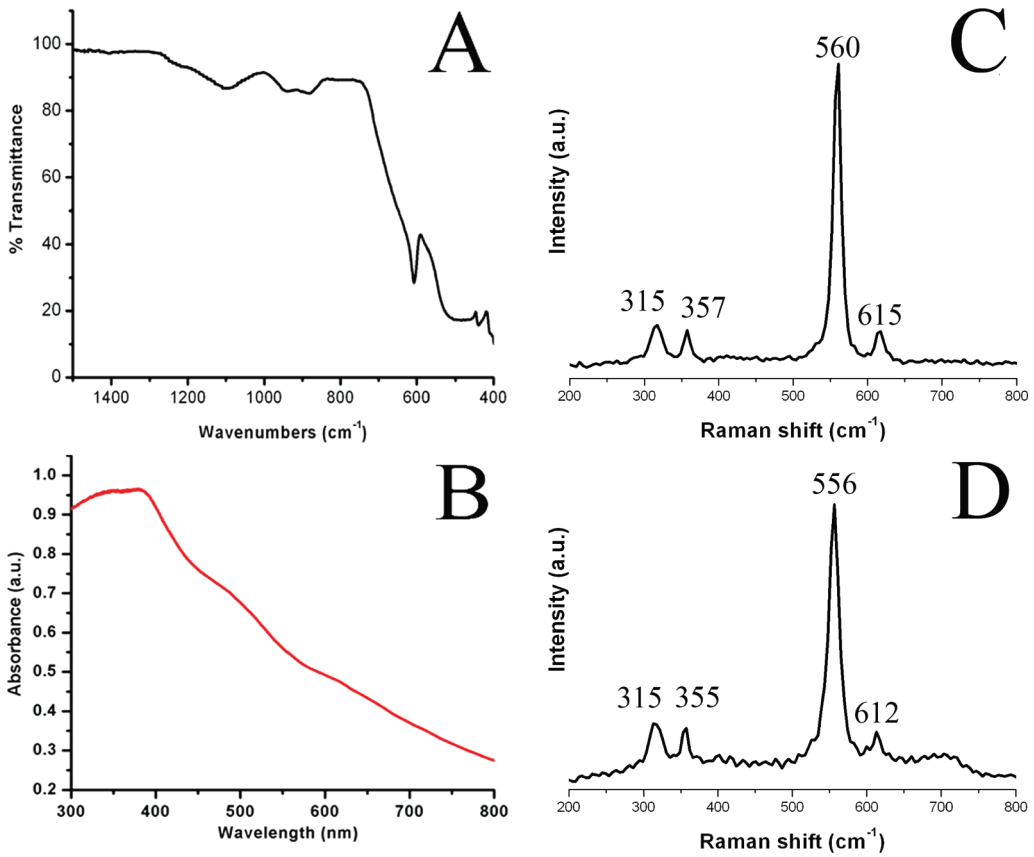

Figure 3. (A) Infrared data and (B) corresponding UV−visible spectrum of Cr_2O_3 nanowires. Raman spectrum of (C) bulk Cr_2O_3 and of (D) Cr_2O_3 nanowires.

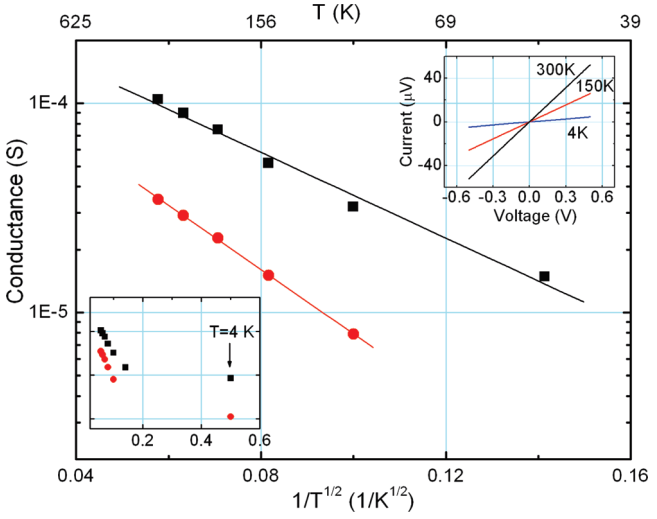

Figure 4. Temperature dependence of the conductance from ~50 to 300 K for two nanowires: A (black squares) and B (red dots). Solid lines are fits to the form of $\sigma \propto \exp(T_0/T)^{1/2}$. Top inset: Current−voltage curves measured at three temperatures for nanowire A (nanowire B showed similar results). Bottom inset: Same as main graph but including points measured at 4 K. The graph shows the onset of a distinct transport mechanism for temperatures below 50 K.

vibrational mode of A_{1g} symmetry, whereas all remaining, noticeable peaks can be attributed to E_g symmetry.[48,49]

Figure 4 shows the conductance, extracted from the $C-V$ curves, as a function of temperature in the ~50−300 K range. A thermal activation conductance of the form, $\sigma \propto \exp(-E_A/k_BT)$, where E_A is the activation energy and k_B is the Boltzmann constant, does not fit well the data of nanowire A (black squares). Instead, the data for both nanowires fit well the general hopping form, $\sigma \propto \exp(T_0/T)^n$. As a reference, data are plotted using $n = 1/2$, which is the expected exponent for variable-range hopping in 1D.[50] However, due to the limited variation of the conductance in this temperature range, there is a large uncertainty in the value of the exponent. More detailed measurements are needed to clearly identify the kind of hopping conduction in these nanowires. The lower inset of Figure 4 shows that the conductance at 4 K does not follow the same dependence on temperature as the data at higher temperatures, indicating the existence of two distinctive electron transport mechanisms for temperatures above and below ~50 K. This temperature-dependent conductivity behavior down to approximately 50 K has been previously ascribed to the presence of a hopping mechanism for electrons between the Cr^{3+} and Cr^{2+} oxidation states, perhaps attributed to the formation of ferromagnetic spinel Cr_3O_4 impurities.[51] While this explanation may be valid for our system, another option we delve into more deeply later in the manuscript to account for the observed data is the possibility of uncompensated

(49) Mougin, J.; Le Bihan, T. L., G. *J. Phys. Chem. Solids* **2001**, *62*, 553–563.
(50) Mott, N. F.; Davis, E. A. *Electronic Process in Non-Crystalline Materials*; Clarendon Press: Oxford, 1979.
(51) Borisov, P.; Hochstrat, A.; Shvartsman, V. V.; Kleemann, W.; Eimuller, T.; Rodriguez, A. F. *Ferroelectrics* **2008**, *370*, 147–152.

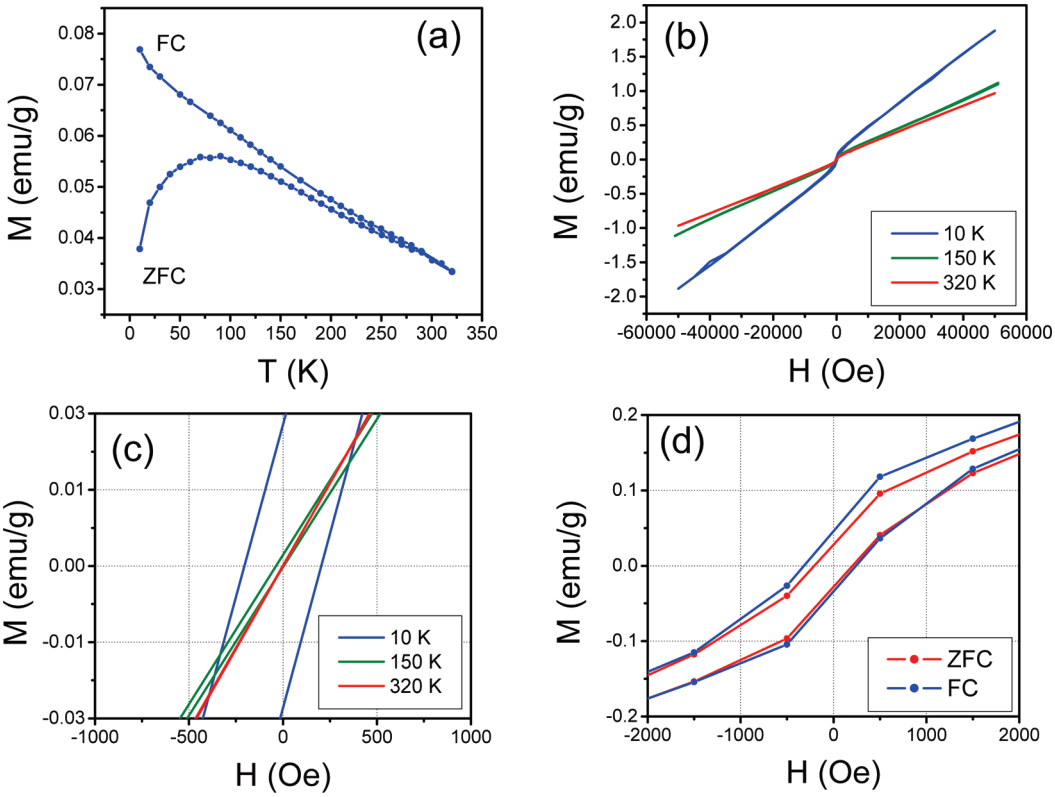

Figure 5. (A) Temperature dependence of FC and ZFC magnetizations at an applied field of 500 Oe; (B) the magnetic field dependence of magnetization at 10, 150, and 320 K; (C) identical to (B) but obtained at low magnetic fields; (D) magnetic field dependencies of ZFC and FC magnetizations taken at 10 K. The FC magnetization was obtained by cooling the sample from 350 to 10 K in an applied magnetic field of 50 kOe.

surface spins. Nevertheless, previous studies on thin film and bulk chromium oxide systems have yielded similar results, though the inflection point in the transition temperature was closer to ~200 K as opposed to 50 K.[51,52] It may also be noteworthy that no magnetoresistance was observed at 4 K in these nanowires for fields of up to 1 T.

III. Magnetic Measurements. The results of magnetization measurements are summarized in Figure 5. The zero-field cooled (ZFC) and field cooled (FC) magnetizations measured at an applied magnetic field of 500 Oe coincide at high temperatures (Figure 5A) but separate below the blocking temperature of about 290 K. While antiferromagnetic order is first observed in bulk Cr_2O_3 at its Néel temperature, T_N = 308 K, there is no sign of either a peak or slope change in the magnetization that would identify T_N in our Cr_2O_3 nanowires. This is not unexpected, since there is only a ~10% reduction of T_N to 270 K in spherical 7.8 nm nanoparticles,[53] where finite size effects may play a much more profound role than in our 179 nm nanowires. The TEM images of our nanowires indicates the presence of substructure, but the large magnitude of the blocking temperature, T_B, which is normally linearly proportional to the nanoparticle volume, indicates that the length scale controlling the magnetic behavior is much larger in our samples than in 15 nm nanoparticles (T_B = 160 K)[54] or in 7.8 nm particles (T_B = 28 K).[53]

The field-dependent magnetization measured at 10, 150, and 320 K is consistent with the presence of a composite magnetic structure within the nanowires, consisting of (i) unsaturated moments which lead to the linear, paramagnetic contribution to the magnetization (Figure 5B) and (ii) saturated moments, which can yield a closed ferromagnetic loop with nonzero coercive field below the blocking temperature (Figure 5C). Such magnetic behavior can be explained by the presence of uncompensated spins at the surface of Cr_2O_3 nanowires, as has been previously reported for Cr_2O_3 nanoparticles.[14,15,37,38] In nanostructures, the uncompensated surface spins possess a lower coordination number. Therefore, a net magnetic moment can be induced on the surfaces of either nominally nonmagnetic nanowires or antiferromagnetic nanoparticles.[55−57]

To further probe the effect of the surface spins, we have tested for the possibility of an exchange bias effect in Cr_2O_3 nanowires.[58,59] Conventionally, the exchange bias effect

(52) Cheng, C.-S.; Gomi, H.; Sakata, H. *Phys. Status Solidi A* **1996**, *155*, 417–425.
(53) Tobia, D.; Winkler, E. L.; Zysler, R. D.; Granada, M.; Troiani, H. E *J. Alloys Compd.* **2010**, *495*, 520.
(54) Makhlouf, S. A. *J. Magn. Magn. Mater.* **2004**, *272−276*, 1530.
(55) Morales, M. P.; Serna, C. J.; Bodker, F.; Morup, S. *J. Phys.: Condens. Matter* **1997**, *9*, 5461.
(56) Teng, X.; Feygenson, M.; Wang, Q.; He, J.; Du, W.; Frenkel, A. I.; Han, W.; Aronson, M. C. *Nano Lett.* **2009**, *9*, 317.
(57) Feygenson, M.; Kou, A.; Kreno, L. E.; Tiano, A. L.; Patete, J. M.; Zhang, F.; Kim, M. S.; Solovyov, V.; Wong, S. S.; Aronson, M. C. *Phys. Rev. B* **2010**, *81*, 014420.
(58) Nogues, J.; Schuller, I. K. *J. Magn. Magn. Mater.* **1999**, *192*, 203.
(59) Nogues, J.; Sort, J.; Langlais, V.; Skumryev, V.; Surinach, S.; Munoz, J. S.; Baro, M. D. *Phys. Rep.* **2005**, *422*, 65–117.

can be observed in composite nanostructures simultaneously possessing both ferromagnetic (FM) and antiferromagnetic (AFM) components with a common interface, such as, for example, in ferromagnetic-core/antiferromagnetic-shell nanoparticles.[59,60] In these nanostructures, the exchange interactions between the FM and AFM parts can lead to a shift of the hysteresis loop along the field axis, once the system has been field cooled. The absolute value of the loop shift is known as the exchange bias field, $\mathbf{H}_{EB}$.

Such a nonzero exchange bias field can also be observed in single phase nanostructures, including in Cr_2O_3 nanoparticles.[15,38] In the case of antiferromagnetic nanoparticles, the exchange bias field would be a result of the exchange interactions between uncompensated surface spins, which play the role of the FM domain, and the AFM core interior of the nanoparticle. As such, we measured the hysteresis loop of Cr_2O_3 nanowires at 10 K, after cooling down from 350 K in an applied field of 50 kOe, and compared our data with zero-field data (Figure 5D). An apparent shift of the FC hysteresis loop is clearly observed with $\mathbf{H}_{EB}$ = 60 Oe. This value is much smaller than those reported for Cr_2O_3 nanoparticles.[53,54] It is possible that there is an element of disorder in the interface between the antiferromagnetic core and the uncompensated surface moments. Alternatively, the thickness of the surface layer is very small, and the exchange coupling to the antiferromagnetic core may simply be too large to allow for the independent reorientation of the shell that lies at the heart of the exchange bias effect. Finally, we cannot rule out the possibility that we are not observing an exchange bias effect at all but rather the formation of an antiferromagnetic substructure in an antiferromagnetic particle, as has been observed in other systems such as NiO.[61,62] We conclude that the magnetism of these Cr_2O_3 nanowires has all the complexity and subtlety expected of a nanoparticle system. The overall promise of this system for combined electronic and magnetic functionality renders it pressing to carry out parametric studies with the goal of determining the fundamental limits of these behaviors.

IV. Effect of Cr_2O_3 on the Thermal Decomposition of $KClO_4$. We have performed catalysis with our metal oxide nanowires. Specifically, we have used these nanostructures for the decomposition of $KClO_4$ into ClO_3^- ions and oxygen. It has previously been shown that due to its $p-n$-type properties as well as its high electronegativity, Cr_2O_3 can effectively lower the thermal decomposition temperature of $KClO_4$ by favoring certain novel mechanistic pathways.[63] As such, Figure 6 shows individual TGA plots of the decomposition of pure $KClO_4$, as well as of $KClO_4$ mixed with bulk Cr_2O_3 and with our Cr_2O_3 nanowires. We have found that both our nanowires and the bulk induce a lower decomposition temperature of $KClO_4$ as compared with pure $KClO_4$ alone. Furthermore, the shoulder present in the data corresponding to both the bulk and nanowire systems can be attributed to formation of $K_2Cr_2O_7$, whereas the small hump present near the tail of the TGA plot can be ascribed to the production of KCl salt.[63]

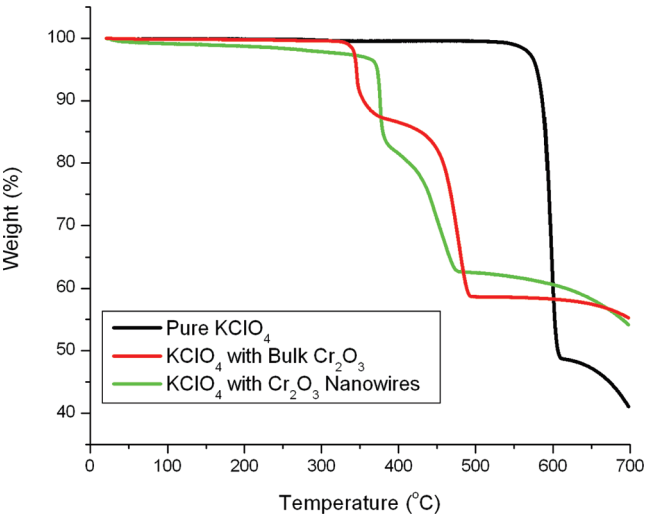

Figure 6. Thermal decomposition of pure $KClO_4$ (black), $KClO_4$ in the presence of bulk Cr_2O_3 (red), and $KClO_4$ in the presence of Cr_2O_3 nanowires (green).

V. Conclusions. In this work, we were able to synthesize one-dimensional chromium oxide (Cr_2O_3) nanowires using a sol−gel technique mediated using a polycarbonate template. The resulting nanowires are crystallographically pure and consist of smaller component nanoparticles that appear to be fused together so as to form a larger 1D motif. The key point is that this high-yield, low-waste synthesis method is a distinct improvement upon previous efforts in that (i) we do not require the use of either specialized or inert gases; (ii) we do not necessitate any particular high-temperature annealing treatment; (iii) our reaction times are reasonably rapid; and (iv) our precursors do not involve hydrazine, supercritical fluids, or any particularly hazardous reaction conditions.

Both magnetic and electronic data have been collected to investigate the properties of as-prepared nanowires. From the former, we conclude that uncompensated surface spins coupled by the exchange interactions to the interior of the nanowires play a dominant role in the magnetic properties of Cr_2O_3 1D nanostructures. From the latter, it was evident that as-prepared nanostructures evinced temperature-dependent conductivity trends, analogous to what has been observed for bulk and thin film analogues. Moreover, the addition of our Cr_2O_3 nanostructures effectively induced the decomposition of a model compound, $KClO_4$, to a much lower decomposition temperature as compared with its pure, uncatalyzed form.

(60) Inderhees, S. E.; Borchers, J. A.; Green, K. S.; Kim, M. S.; Sun, K.; Strycker, G. L.; Aronson, M. C. *Phys. Rev. Lett.* **2008**, *101*, 117202.
(61) Feygenson, M.; Kou, A.; Kreno, L. E.; Tiano, A. L.; Patete, J. M.; Zhang, F.; Kim, M. S.; Solovyov, V.; Wong, S. S.; Aronson, M. C. *Phys. Rev. B* **2010**, *81*, 14420.
(62) Kodama, R. H.; Makhlouf, S. A.; Berkowitz, A. E. *Phys. Rev. Lett.* **1997**, *79*, 1393.
(63) Said, A. A.; Hassan, E. A.; El-Salaam, K. M. A. *Surf. Technol.* **1983**, *20*, 131–137.

Acknowledgment. We thank Hongjun Zhou for helpful discussions. We acknowledge the U.S. Department of Energy (DE-AC02-98CH10886) for facility (including microscopy) and personnel (including PI) support. S.S.W. also thanks the Alfred P. Sloan Foundation for experimental supplies necessary for the synthesis reactions.

Supporting Information Available: Figure showing the formation of nanoparticles after the template was cleaned with a Kimwipe and SEM image of as-prepared nanowires of different diameters, fabricated using a polycarbonate template (PDF). This material is available free of charge via the Internet at http://pubs.acs.org.